Neuron
Report

Optogenetic Inactivation Modifies Monkey Visuomotor Behavior

James Cavanaugh,[1,4,*] Ilya E. Monosov,[1,4] Kerry McAlonan,[1] Rebecca Berman,[1] Mitchell K. Smith,[1] Vania Cao,[2] Kuan H. Wang,[2] Edward S. Boyden,[3] and Robert H. Wurtz[1]
[1]Laboratory of Sensorimotor Research, National Eye Institute, NIH, Bethesda, MD 20982-4435, USA
[2]Unit on Neural Circuits and Adaptive Behaviors, Genes Cognition and Psychosis Program, National Institute of Mental Health, NIH, Bethesda, MD 20892, USA
[3]Department of Biological Engineering and Brain and Cognitive Sciences, MIT, Cambridge, MA 02139, USA
[4]These authors contributed equally to this work
*Correspondence: jrc@lsr.nei.nih.gov
http://dx.doi.org/10.1016/j.neuron.2012.10.016

SUMMARY

A critical technique for understanding how neuronal activity contributes to behavior is determining whether perturbing it changes behavior. The advent of optogenetic techniques allows the immediately reversible alteration of neuronal activity in contrast to chemical approaches lasting minutes to hours. Modification of behavior using optogenetics has had substantial success in rodents but has not been as successful in monkeys. Here, we show how optogenetic inactivation of superior colliculus neurons in awake monkeys leads to clear and repeatable behavioral deficits in the metrics of saccadic eye movements. We used our observations to evaluate principles governing the use of optogenetic techniques in the study of the neuronal bases of behavior in monkeys, particularly how experimental design must address relevant parameters, such as the application of light to subcortical structures, the spread of viral injections, and the extent of neuronal inactivation with light.

INTRODUCTION

A major goal of systems neuroscience is to identify brain mechanisms responsible for specific behaviors. Correlation of neuronal activity to behavior led the way to the identification of neuronal circuits underlying a wide range of sensory, motor, and cognitive behaviors in the primate model of human behavior. But linking neuronal activity to behavior requires another step: showing that modifying neuronal activity actually changes behavior.

Localized and reversible chemical inactivation of neurons is now widely used as a key test of which neuronal circuits underlie specific behaviors. Inactivation with anesthetics (such as lidocaine) or inhibitory transmitter agonists (such as muscimol) have been particularly useful because such inactivations last minutes to hours, so the activity of the brain during inactivation can be tested before behavioral adaptation to the resulting deficit occurs. A substantial limitation of chemical inactivation, however, is that the effects persist until the drug is metabolized, and comparing its effects to a control condition on a trial-by-trial basis is impossible.

The recent introduction of optogenetic tools offers solutions to these limitations. Genetically encoded molecules target specific neurons in the brain, and enable their activity to be modulated by light. Optogenetic inactivation (as well as activation), developed primarily in rodents, has been effective in modifying behavior in vivo as shown in many studies (Knöpfel and Boyden, 2012; Tye and Deisseroth, 2012). Optogenetic techniques have also been implemented in monkeys, and the effectiveness of these techniques in turning on or off neurons has been amply demonstrated (Diester et al., 2011; Han et al., 2011; Han et al., 2009). However, experimentally changing monkey behavior by optogenetic techniques has remained elusive. Diester et al. (2011) tried to modify skeletal motor behavior by stimulating motor and somatosensory cortex of macaque monkeys using channel rhodopsin but found neither modulation of spontaneous activity of the resting arm and hand, nor an effect of optical stimulation with simultaneous electrical stimulation of motor and somatosensory cortex.

We reasoned that a more sensitive measure of behavior might show effects of optogenetic manipulation. We decided to determine if optogenetic manipulation of neurons within the superior colliculus (SC) could influence visually guided saccadic eye movements, which can be measured with great precision. Neurons at a given location in the intermediate layers of the SC discharge before saccades to a given region of the visual field, and their chemical inactivation alters the endpoint, velocity, and latency of these saccades. Furthermore, these neurons are organized into a precise representation of the visual field (Robinson, 1972), so we can predict exactly where in the visual field changes in neuronal activity should produce changes in behavior. We therefore introduced the light-driven outward proton pump ArchT (Chow et al., 2010; Han et al., 2011) into SC intermediate layer neurons. We found that optogenetically inactivating these SC neurons produced clear and repeatable deficits in saccades. We have used these deficits along with the SC map to explore the advantages and limitations of optogenetic modulation of monkey behavior.

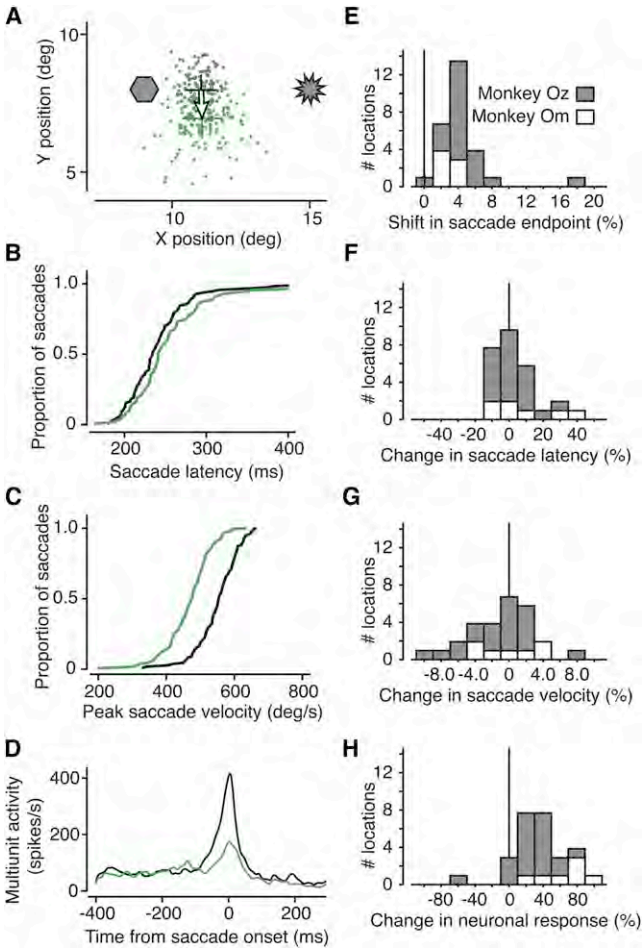

Figure 1. Behavioral Effects from Optogenetic Control

(A) Saccades with and without laser stimulation directed to a visual target at 11.5°, 8.0°. Saccade endpoints are shown without (gray) and with (green) laser stimulation. Laser light was introduced into the intermediate layers of the SC on randomly interleaved trials. This was done by opening and closing a fast shutter placed in the path of the laser, which remained on throughout the experiment. Green and black crosses indicate the mean saccade endpoints (±1 SEM) with and without light, respectively. This example was chosen as a clear demonstration, but most results were based on fewer trials. (B) Cumulative distribution of saccade latencies for this example. Black are latencies without light, green are in the presence of laser light. (C) Cumulative distributions of peak saccade velocity. The green trace shows peak velocity in the presence of laser light, and the black trace is without light. (D) Multiunit neuronal activity with and without laser stimulation for this example. Neuronal responses are shown as spike density histograms aligned to saccade onset at time zero and smoothed with a Gaussian filter with a 5 ms SD. Changes in neuronal activity were not related to shifts in saccade endpoint (see Figure S1). (E–H) Distributions of these effects for 28 experiments in two monkeys.

RESULTS

We studied optogenetic inactivation of one side of the SC in three monkeys. We injected an adenoassociated virus (AAV) incorporating ArchT fused to GFP (Han et al., 2011) and expressed under a pancellular promoter (CAG), into the intermediate layers of the SC. Neurons in these layers discharge before saccades and their chemical inactivation produces deficits in saccades. At least 6 weeks after the injection of the virus, we tested the effect of shining green laser light (532 nm wavelength) onto these SC neurons. In two monkeys (OZ and OM), we presented the laser light while the monkey made visually guided saccades. In the third monkey (RO), we studied changes in neuronal responses during free viewing. The light reached the SC typically via a 200 μm diameter optic fiber attached to a recording electrode extending 500 μm beyond the flat fiber end (the optrode).

Modification of Saccadic Behavior

We found consistent behavioral effects in monkeys OZ and OM using laser light inactivation. Visually guided saccades showed the same triad of effects as with chemical inactivation: shift in saccadic end point, reduced peak velocity, and increased latency. Figure 1 shows the effects of laser inactivation at an example site in monkey OZ. We located the optrode in the SC intermediate layers during each experiment by the center of the movement fields represented by neuronal activity recorded 500 μm below the fiber tip. While the monkey fixated a central bright spot on a dark background, we presented a second spot of light and the monkey was rewarded for making a visually guided saccade to that spot once the fixation spot disappeared.

Figure 1A shows the locations in the visual field of the ArchT injection site (hexagon) and the optrode (starburst). Gray points are the endpoints of normal saccades to the visual target. Green points are saccade endpoints to the same visual target during SC inactivation. Saccade endpoints shifted on average about 1.02° down in this example (shown by the arrow), or about 7.3% of the saccade magnitude. These distributions of saccade endpoints were significantly different with and without light (2D Kolmogorov-Smirnov [KS] test, $p < 0.001$).

We did not methodically study the effect of laser intensity on behavior. However, we were of course able to eliminate any change in behavior by sufficiently turning down the laser from our default intensity of about 650 mW/mm^2. Effects at less than 300 mW/mm^2 were negligible if present at all. Also, at several stimulation sites where we tested multiple laser intensities, we could not further increase the magnitude of the saccadic shift by increasing laser illumination, even up to 1600mW/mm^2.

In addition to changing the endpoints of saccades, photostimulation changed saccade latency and peak velocity. Figure 1B shows the cumulative distribution of saccade latencies without (black) and with (green) laser light. The distribution was shifted to the right with light, an increase of about 7 ms in saccade latency ($p = 0.020$, Wilcoxon rank-sum test). Figure 1C shows that the light shifted the distribution of peak saccade velocities to the left, a significant reduction in peak velocity of about 79°/s ($p < 0.001$, t test). Note that subsequent p values without a specified test were obtained from a t test.

Figure 1D shows neuronal activity as spike density histograms, aligned to saccade onset. At this optrode location in the SC, multiunit activity representing the burst before the saccade decreased more than 60% with laser illumination, indicating a clear neuronal correlate for the behavioral changes we observed in saccade endpoint, saccade velocity, and saccade latency.

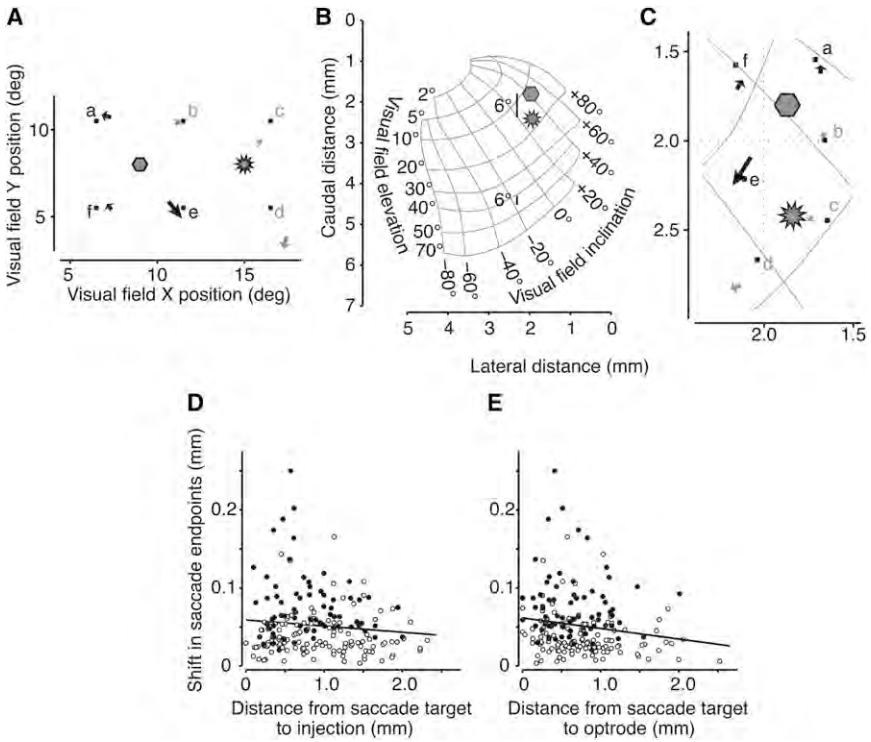

Figure 2. Magnitude of Saccadic Shift Diminishes with Distance from Both Injection and Laser Illumination

(A) Locations of the six targets in the visual field (small squares) along with the location of the injection site and the optrode site. Arrows show the shift in mean saccade endpoint when the SC was exposed to light. Significant shifts are plotted in black (gray otherwise). (B) Location on the collicular map of the injection (hexagon) and optrode (starburst) from the locations in (A). Bars subtending 6° of visual angle are shown for central and peripheral visual field locations to illustrate magnification within the SC map. (C) Region of interest on the SC map showing the injection, optrode, saccade targets, and shifts in saccade endpoints. Significant shifts are shown in black, gray otherwise. (D) Shift magnitude plotted against distance from injection. Both quantities are expressed as mm in the SC. Solid points denote significant shifts, whereas open symbols are not significant. The solid black line is the least-squares linear fit to all the data. (E) Shift magnitude plotted against distance from optrode. Symbols are the same as in (D).

Figures 1E–1H show the distributions of the above effects for 28 experiments. For the 21 experiments in OZ and the 7 in OM, the only difference between the monkeys was the reduction in neuronal response (most likely due to the fact that responses in monkey OM were recorded from single units, whereas in monkey OZ we predominantly recorded multiunit activity). For monkey OM, neuronal responses were reduced 68.2% on average ($p < 0.001$) and in monkey OZ 27.4% ($p < 0.001$). Saccade endpoints shifted an average of 4.6% of the saccade magnitude ($p < 0.001$, 2D KS test), latency increased 7.3 ms ($p = 0.20$, rank-sum test), and saccade velocity was reduced by 9.6°/s ($p = 0.29$). As expected, there was no relationship between the changes in neuronal activity and changes in saccade endpoint (see Figure S1 available online).

In summary, we show that optogenetic inactivation of a region of the SC produced changes in saccades made to targets in the visual field near that same SC region. The shift in saccade endpoint and the changes in saccade peak velocity and latency were consistent with the deficits found with chemical inactivation (Hikosaka and Wurtz, 1985, 1986).

Relating the Magnitude of Shifts in Saccade Endpoint to Injection and Optrode Locations

A major advantage of testing optogenetic techniques in the monkey SC is that the locations of certain variables of interest, namely the shift in saccade endpoint, the location of the injection and the location of the optrode can all be represented on the same retinotopic map. This allows us to quantitatively evaluate how the spatial separation between the injection, the laser, and the active neurons affects the strength of optogenetic manipulations.

We presented saccade targets to monkey OZ at different locations in the visual field on randomly interleaved trials while the location of the injection and the optrode remained constant during an experiment. Figure 2 shows results from such an experiment (same optrode site as in Figure 1). On each trial we presented one of several targets, in this case six, distributed around both the injection site and the optrode site (Figure 2A). As before, the arrows show how the endpoints of saccades to each target shifted with light inactivation. Black arrows denote significant shifts, and gray arrows show those not reaching significance (2D KS test, $p < 0.01$). Changes in the saccade endpoints varied among targets in both direction and magnitude of the shift.

The first question is whether the magnitude of the behavioral effect (the shift in saccade endpoint) had any relation to the saccade target's distance from either the injection site or the optrode. The proper frame of reference to answer such questions is in the SC because the injection, the laser light, and the active neurons are each defined within the SC rather than the visual field, which is distorted by a magnification factor. This can be seen in Figure 2B which shows how 6° in the visual field (the distance between the injection site and this optrode site) subtends different distances on the SC depending on eccentricity. Also shown in Figure 2B are the same locations of the injection and optrode from Figure 2A on the SC map of the visual field. We have enlarged this region in Figure 2C to include the locations of the saccade targets and the shifts in saccade endpoint.

For 199 targets from 21 experiments in monkey OZ we have plotted in Figure 2D the magnitude of the shift in saccade endpoint against the distance from each target to the injection site (t-inj). There was a minor trend for the magnitude of the

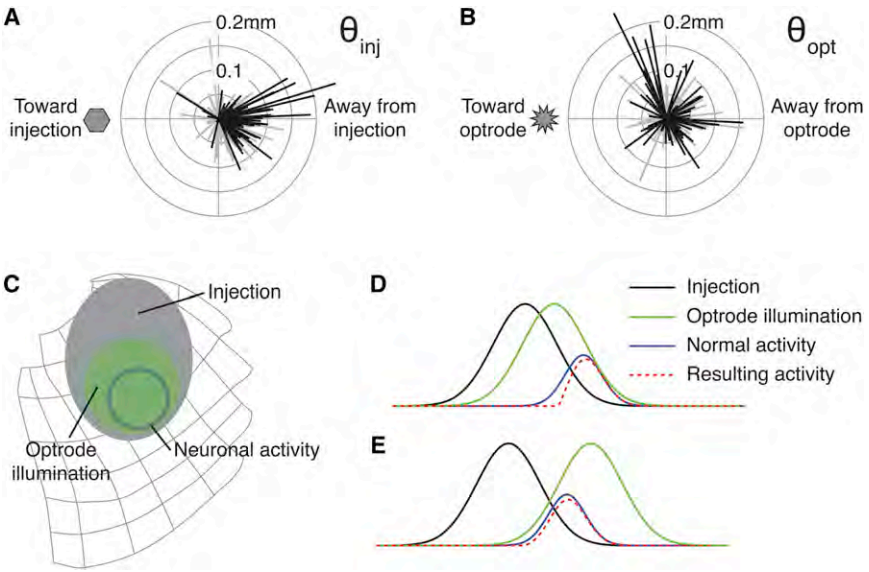

Figure 3. Saccades Are Deflected Away from the Injection, Not the Laser

(A) Shifts in saccade endpoints relative to the injection site for 199 separate targets from all experiments. (B) Shifts in saccade endpoints relative to the optrode site from all experiments. (C) Schematic of optogenetic influence of laser illumination on saccade-related neuronal activity in the SC. The gray ellipse is the proposed extent of the injection. The solid circle is the presumed population of neurons active during a saccade to a target about 12° to the right. The green superimposed on both shows the region supposedly illuminated by the laser. (D) Schematic of optogenetic influence in one dimension. The regions from (C) are now shown as Gaussian curves. When the laser (green curve) is positioned between the injection site (black curve) and the active neurons (blue curve), a subpopulation of neurons are inactivated, resulting in the neuronal activity represented by the dashed red curve, shifted away from the injection. (E) Distal placement of the laser still results in shifts away from the injection. See also Figure S2.

behavioral effect to reduce as t-inj increased ($r = -0.12$, $p = 0.12$). Figure 2E shows the same endpoint shifts as in Figure 2D, this time plotted against the distance on the SC from the target to the light (t-opt). Again the size of the behavioral effect was less for saccades more distant from the optrode. The black least-squares line to the data confirms this small trend ($r = -0.16$, $p = 0.02$). We must note, however, that there was a similar relationship between the shift in saccade endpoint and the magnitude of the saccade, t-ecc ($r = -0.11$, $p = 0.12$).

To determine the relative contributions of these three distances (t-inj, t-opt, t-ecc), we performed a multiple linear regression. These three factors sufficiently predicted the behavioral effect ($F = 3.7012$, $p = 0.0063$) although the distance from the target to the laser, t-opt, dominated the regression (coefficients: t-opt = -0.021, $p = 0.002$; t-inj = -0.005, $p = 0.320$; t-ecc = -0.001, $p = 0.0254$).

In summary, the magnitude of the primary change in behavior we measured, the shift in saccade endpoint, was related to the proximity of both the injection site and the optrode site to the SC neurons underlying the saccade. However, these distances were not independent during an experiment, and further analysis showed that the magnitude of the saccadic shift was predominantly dependent on proximity to the laser illumination.

Relating the Direction of Shifts in Saccade Endpoint to Injection and Optrode Locations

Each shift in saccade endpoint was in a specific direction on the visual field map (Figure 2C). The next question was whether the directions of these shifts had any relation to either the location of the injection or the location of the laser light.

The first angle of interest θ_{inj} represents the direction of the mean shift in saccade endpoints relative to the injection site (see Figure S2). In short, if saccades shifted directly away from the injection site, θ_{inj} would be 0° (directly to the right in Figure 3A) whereas 180° (or −180°) would be directly toward the injection site (directly to the left). We calculated θ_{inj} for saccades to each of the targets in each experiment. For 21 experiments in monkey OZ, Figure 3A shows the relative displacement vectors from the injection site for saccades to every target. Significant shifts are shown in black. Shifts in saccade endpoints were predominantly away from the injection site.

We performed this analysis again, this time measuring how saccade endpoints shifted away from the site of laser light, calculating the corresponding angle θ_{opt}. Figure 3B shows these shifts for all experiments. The pattern of shifts away from the laser is noticeably different than the shifts away from the injection site.

To summarize the selectivity of the directions of shifts we used a polar selectivity measure derived from the circular mean vector (Cavanaugh et al., 2002; Leventhal et al., 1995) in which we normalized the vector sum of the shifts by the sum of the shift magnitudes (see Supplemental Experimental Procedures). The angle of the resultant vector indicates the mean displacement direction. The magnitude of this vector is the degree of selectivity (0 for no selectivity to 1 for perfect selectivity). Significant deflections away from the injection site had a selectivity index of 0.765 at −10.5° (where 0° is directly away from the injection). Significant deflections away from the optrode had a selectivity index less than half that (0.37) at an angle of 31.4°. For all displacements, significant and nonsignificant, selectivity away from the injection site was 0.627 at −9.6°, whereas selectivity away from the optrode site was just 0.209 at 41.8°. In summary, these results demonstrate that saccades were more consistently and selectively deflected away from the injection site than away from the optrode site.

We believe this effect can be understood intuitively by considering three gradients: the gradient of the virally transfected neurons around the SC injection site, the gradient of light intensity around the optrode, and the gradient in the strength of neuronal activity with saccades made to a given target. These three regions are schematically illustrated on the map of the

SC in Figure 3C. The extents of the regions in this qualitative analysis are based on the areas we have observed in our experiments. We have taken these gradients into a single dimension in Figure 3D. Here each gradient is represented as a Gaussian curve. In this example, we have placed the optrode between the center of the injection and the saccade target. The dashed red curve shows the resultant neuronal activity according to a simple scheme; we multiplied the injection (transfected cells) by the illumination to represent the experimentally affected cells and subtracted this from the normal neuronal activation. When the laser is placed between the injection and the saccade target, neuronal activity is slightly shifted away from the injection, which would cause a small shift in saccades away from the injection site. In Figure 3E, the laser illumination has been placed on the other side of the target. The resulting neuronal activity is once again shifted slightly away from the injection, not the optrode, consistent with our observations. In net, we envision the effect of illumination on the gradient of transfected cells as being akin to shining a spotlight on a hillside. The light illuminates the slope of the hill, which defines the gradient of the shift in neuronal activity and the resulting shift in saccade endpoint.

Area of Neuronal Sensitization Measured by Neuronal Suppression

Behavioral changes give us some idea of the spatial spread of the optogenetic influence, but saccades are defined by the activity of a population of neurons that can span millimeters in the SC (1.4 mm estimated for SC burst cells; Munoz and Wurtz, 1995). Also, from Figure 2E, the laser illumination from the optrode could be affecting neurons over a millimeter away. A better estimate of the extent of sensitized neurons can be derived from the suppression of neuronal responses, the detection of which is limited to few hundred microns from the optrode. We pursued this in two monkeys, OZ and RO, making an effort to sample SC sites beyond the presumed center of the injection.

We used the established map of saccade directions and amplitudes across the intermediate layers of the SC to determine each optrode location, and characterized the degree to which we could affect neuronal responses with light at that location. We calculated the maximum reduction in response at each optrode site and produced a map by interpolating between the irregularly spaced data. Figure 4 shows the maps for the two monkeys. The area of the injection in OZ (Figure 4A) was clearly delineated at the lateral edge of the interpolated region where response differences diminished (whiter areas). We estimated the spread of the effect by fitting a two-dimensional Gaussian curve to the responses. The Gaussian was free to vary its center, orientation, height, and extent. We show the extent of the Gaussian (±1 SD along each axis) as the dashed ellipse in Figure 4A. The region measured approximately 2,700 μm long by 2,100 μm across. For monkey RO (Figure 4B) the red ellipse indicates the actual extent of transfected neurons obtained from the histological evaluation described below.

Area of Neuronal Transfection Measured by Histological Reconstruction

Figure 4C shows how we constructed a three-dimensional representation of the injection in monkey RO from histological sections. Our histological methods are explained in detail in Supplemental Experimental Procedures. For each of 11 coronal sections separated by 250 μm, we obtained the total number of neurons by counting the cells expressing the NeuN stain. We then counted which neurons expressed GFP, indicating transfection with the ArchT construct (see Figure S3). The marginal histograms in Figure 4C are simply the running means of the proportion of transfected cells in each section. Over the 11 sections, we used the extent of each running mean to establish the anterior-posterior and medial-lateral spread of the transfection. The central wireframe structure schematizes the three-dimensional reconstruction of the spread of the virus in monkey RO.

From our reconstruction, the injection extended approximately 2,500 μm along the anterior-posterior axis. The maximum extent of the injection along the medial-lateral axis was about 1,200 μm, and the extent along the dorsal-ventral axis was approximately 800 μm. The extent of this region can be seen on the collicular map of monkey RO in Figure 4B as the red dashed ellipse.

The injection shown in the histology was 6 μl (as opposed to 7 μl in monkey OZ). In addition, there is possible tissue shrinkage during processing. These factors may have contributed to the difference between injection spreads in Figures 4A and 4B. Since the tissue was sliced before staining, shrinkage does not apply to the AP dimension, which would contribute to the anisotropy of the injection in Figure 4B. Any residual anisotropy in either monkey could be due to a predominance of fibers in the intermediate layers running in the AP direction (Nakahara et al., 2006).

In summary, using the results from both the area of neuronal suppression within the SC (two monkeys) and the spread of GFP labeled neurons in the SC (one monkey), we estimate that single injection of 6–7 μl effectively sensitizes neurons to light in a region subtending about 2.5 mm by 2.3 mm horizontally.

DISCUSSION

What We Learn from Optogenetic Modulation of Saccadic Eye Movements

Neurons in the monkey have been shown previously to be activated or inactivated using optogenetic techniques (Diester et al., 2011; Han et al., 2009). We have now shown that monkey behavior also can be modified by optogenetic procedures, and described the conditions and parameters that govern success. Saccadic eye movements to visual targets showed the same trilogy of changes (a shift in saccadic endpoint, an increase in latency, and a decrease in velocity) with light-induced inactivation as with inactivation of SC by the anesthetic lidocaine or the GABA agonist muscimol.

These experiments show how the benefits of optogenetic tools translate to the study of primate behavior. First is the ability to have trials in which the target neurons are inactivated interleaved with those in which they are not. This permits comparison of experimental and control trials with only seconds of separation compared to chemical inactivation where control trials come long before or after the experimental trials. Second, there are minimal changes in optogenetic inactivation over a series of trials. In contrast, the effects of drug injections are always

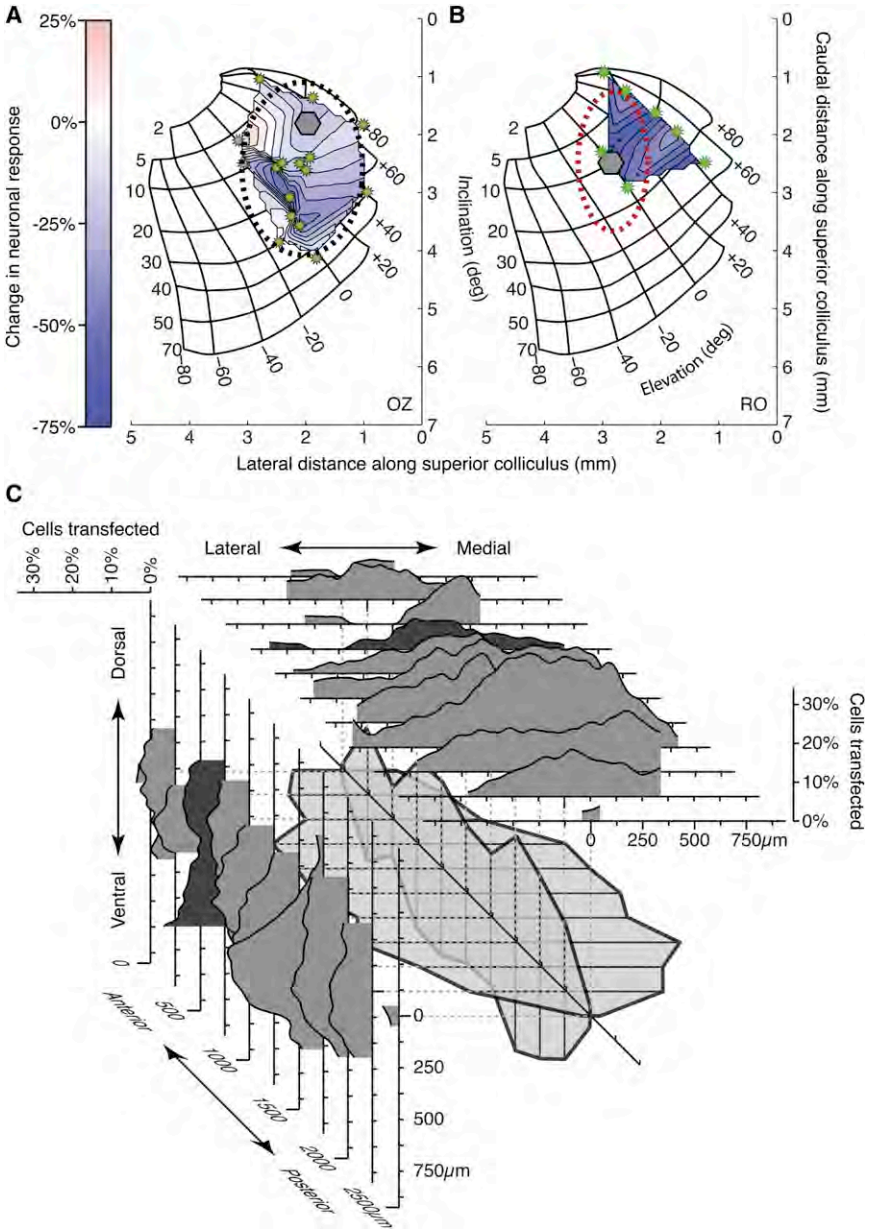

Figure 4. Spread of ArchT Transfection

The suppression of neuronal activity at several sites in the SC is shown for monkey OZ (A) and monkey RO (B). The injection site and optrode locations are shown as the hexagon and the starbursts, respectively. Axes indicate distance in mm along the SC. The color bar to the left shows how greater suppression is indicated by darker blue. Lighter regions in the interpolated area denote little change. The black ellipse shows the estimated extent of light sensitivity in monkey OZ determined by a 2D Gaussian fit to the data. The red ellipse in (B) shows the extent of the injection in Monkey RO determined from subsequent histological analysis. (C) For each of 11 histological sections from monkey RO we constructed marginal density plots (see Supplemental Experimental Procedures) representing the degree of transfection over the X and Y dimensions. Sections are aligned to the centers of their marginal distributions. The extents of transfection from each section have been combined in sequence in the center of the plot, with adjacent sections connected. This wireframe structure represents the spread of transfection in three dimensions. See also Figure S3.

changing due to the spread of the drug and its continual metabolizing. Third, techniques for injection and recording are similar to those already used in most laboratories studying the neuronal bases of behavior. Fourth, once the viral injection is made, localized inactivation can be shifted within the region of transfected neurons by simply moving the optrode, as is illustrated by Figure 4. Finally, the area inactivated can be small enough to produce precise deficits such as those shown for the shifts in saccade endpoints in Figure 3.

For other experiments, however, the small area of inactivation can be a substantial disadvantage. Saccade endpoints shifted on average about 5% of saccade magnitude, which for eye movements is readily measurable. In contrast, initial exploratory evaluation of a certain brain area frequently requires larger regions of inactivation, particularly when the relation of the area to behavior is tenuous. Small changes in behavior in such cases may go undetected, so a larger inactivation would probably be necessary to reveal the contribution of the structure to behavior. The limited size of the inactivation might well have contributed to the lack of any behavioral effect of channel rhodopsin injections made in monkey motor cortex (Diester et al., 2011).

Interaction of Static Injection Location and Movable Light Location

Optogenetic inactivation differs from chemical inactivation in having greater precision and added flexibility. With chemical inactivation, the effect on behavior is dependent on the overlap of the area of neurons active in generating the behavior (in our case a saccade) and the area of neurons inactivated by the chemical. With the optogenetic approach, however, there is a third gradient: the illumination from the optrode on targeted neurons. Essentially, the outcomes and interpretations of each optogenetic experiment are governed by the interaction of these three gradients.

The effect of these gradients on behavior was interesting: size of the effect depended on the saccade's distance from the optrode, and we would expect this factor to govern behavioral effects in any brain area. In addition, we found a systematic change in the direction of this shift that depended on the location of the injection. Saccade related neurons are mapped on the

intermediate layers of the SC as vectors pointing to different regions of the visual field. Activity during a saccade is the result of a large population of such neurons (Munoz and Wurtz, 1995), the average of whose vectors determines the generated saccade (Lee et al., 1988). In fact, the precision of the optogenetic method provides the most convincing evidence so far (Figure 3A) that shifts in saccade endpoints can be predicted if one knows the shift in the vector average resulting from inactivation. In our experiments, the shifts are most easily interpreted as the action of the injection gradient and the light gradient acting on the SC neuronal vector gradient, as indicated by the analysis in Figures 3C–3E.

Although chemical inactivation might well have a place in studying the brain, optogenetic techniques allow a new set of strategies with remarkable temporal and spatial precision, some of the principles of which we have illustrated here.

EXPERIMENTAL PROCEDURES

Three adult male monkeys (OZ, OM, RO; *Macaca mulatta*) provided data for different aspects of these experiments. Monkeys weighed between 8 and 11 kg and had implanted scleral search coils for measuring eye position, had recording cylinders for accessing SC neurons, and had posts for immobilizing the head during experiments as described previously (Sommer and Wurtz, 2000). All procedures were approved by the Institute Animal Care and Use Committee and complied with Public Health Service Policy on the humane care and use of laboratory animals.

Monkeys sat in a primate chair positioned 57 cm in front of a tangent screen. The chair was in a dark room in the center of magnetic field coils used for measuring eye movements. For monkeys OZ and OM, computers running REX (Hays et al., 1982) and associated programs controlled stimulus presentation, administration of reward, the recording of eye movements and single neuron activity, and the on-line display of results. For monkey RO, eye movements and neuronal data were acquired using a Plexon System. Visual stimuli appeared on a gray background on an LCD monitor or were back-projected by an LCD projector. Monkeys were rewarded with drops of fruit juice or water.

See Supplemental Experimental Procedures for further details.

SUPPLEMENTAL INFORMATION

Supplemental Information includes three figures and Supplemental Experimental Procedures and can be found with this article online at http://dx.doi.org/10.1016/j.neuron.2012.10.016.

ACKNOWLEDGMENTS

We are grateful to Altah Nichols and Tom Ruffner for machine shop support and to Kirk Thompson for his efforts in the initial stages of the experiments.

Accepted: October 17, 2012
Published: December 5, 2012

REFERENCES

Cavanaugh, J.R., Bair, W., and Movshon, J.A. (2002). Selectivity and spatial distribution of signals from the receptive field surround in macaque V1 neurons. J. Neurophysiol. *88*, 2547–2556.

Chow, B.Y., Han, X., Dobry, A.S., Qian, X., Chuong, A.S., Li, M., Henninger, M.A., Belfort, G.M., Lin, Y., Monahan, P.E., and Boyden, E.S. (2010). High-performance genetically targetable optical neural silencing by light-driven proton pumps. Nature *463*, 98–102.

Diester, I., Kaufman, M.T., Mogri, M., Pashaie, R., Goo, W., Yizhar, O., Ramakrishnan, C., Deisseroth, K., and Shenoy, K.V. (2011). An optogenetic toolbox designed for primates. Nat. Neurosci. *14*, 387–397.

Han, X., Qian, X., Bernstein, J.G., Zhou, H.H., Franzesi, G.T., Stern, P., Bronson, R.T., Graybiel, A.M., Desimone, R., and Boyden, E.S. (2009). Millisecond-timescale optical control of neural dynamics in the nonhuman primate brain. Neuron *62*, 191–198.

Han, X., Chow, B.Y., Zhou, H., Klapoetke, N.C., Chuong, A., Rajimehr, R., Yang, A., Baratta, M.V., Winkle, J., Desimone, R., and Boyden, E.S. (2011). A high-light sensitivity optical neural silencer: development and application to optogenetic control of non-human primate cortex. Front. Syst. Neurosci. *5*, 18.

Hays, A.V., Richmond, B.J., and Optican, L.M. (1982). A UNIX-based multiple process system for real-time data acquisition and control. WESCON Conference Proceedings *2*, 1–10.

Hikosaka, O., and Wurtz, R.H. (1985). Modification of saccadic eye movements by GABA-related substances. I. Effect of muscimol and bicuculline in monkey superior colliculus. J. Neurophysiol. *53*, 266–291.

Hikosaka, O., and Wurtz, R.H. (1986). Saccadic eye movements following injection of lidocaine into the superior colliculus. Exp. Brain Res. *61*, 531–539.

Knöpfel, T., and Boyden, E.S. (2012). Tools for observing and controlling specific molecular or physiological pathways in intact cells and tissues. Preface. Prog. Brain Res. *196*, vii–viii.

Lee, C., Rohrer, W.H., and Sparks, D.L. (1988). Population coding of saccadic eye movements by neurons in the superior colliculus. Nature *332*, 357–360.

Leventhal, A.G., Thompson, K.G., Liu, D., Zhou, Y., and Ault, S.J. (1995). Concomitant sensitivity to orientation, direction, and color of cells in layers 2, 3, and 4 of monkey striate cortex. J. Neurosci. *15*, 1808–1818.

Munoz, D.P., and Wurtz, R.H. (1995). Saccade-related activity in monkey superior colliculus. II. Spread of activity during saccades. J. Neurophysiol. *73*, 2334–2348.

Nakahara, H., Morita, K., Wurtz, R.H., and Optican, L.M. (2006). Saccade-related spread of activity across superior colliculus may arise from asymmetry of internal connections. J. Neurophysiol. *96*, 765–774.

Robinson, D.A. (1972). Eye movements evoked by collicular stimulation in the alert monkey. Vision Res. *12*, 1795–1808.

Sommer, M.A., and Wurtz, R.H. (2000). Composition and topographic organization of signals sent from the frontal eye field to the superior colliculus. J. Neurophysiol. *83*, 1979–2001.

Tye, K.M., and Deisseroth, K. (2012). Optogenetic investigation of neural circuits underlying brain disease in animal models. Nat. Rev. Neurosci. *13*, 251–266.

Neuron, Volume *76*

Supplemental Information

Optogenetic Inactivation Modifies Monkey Visuomotor Behavior

James Cavanaugh, Ilya E. Monosov, Kerry McAlonan, Rebecca A. Berman, Mitchell K. Smith, Vania Cao, Kuan H. Wang, Edward S. Boyden, and Robert H. Wurtz

SUPPLEMENTAL INFORMATION INVENTORY

Supplemental Data

Supplemental Experimental Procedures

Laser stimulation

In this section we describe our custom optrode for simultaneous neuronal recording and photostimulation. We specify the laser and shutter hardware used and relate the parameters used for photostimulation.

Histology

We give a detailed description of all processes involved in tissue fixing and immunohistochemistry.

Confocal microscopy and cell counting

We present in detail the procedures related to cell counting and the determination of transfection.

Supplemental References

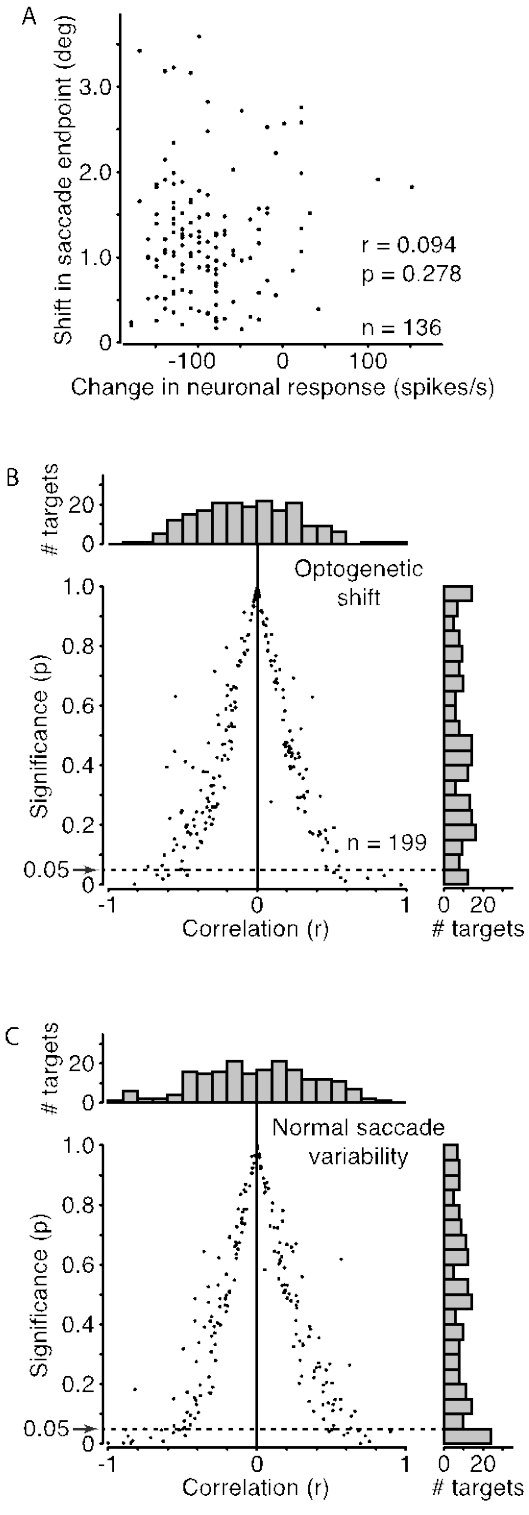
A
Shift in saccade endpoint (deg)
3.0
2.0
1.0
0
r = 0.094
p = 0.278
n = 136
-100
0
100
Change in neuronal response (spikes/s)
B
targets
20
0
Optogenetic
shift
1.0
0.8
0.6
0.4
0.2
0.05
0
Significance (p)
n = 199
-1
0
1
Correlation (r)
0 20
targets
C
targets
20
0
Normal saccade
variability
1.0
0.8
0.6
0.4
0.2
0.05
0
Significance (p)
-1
0
1
Correlation (r)
0 20
targets

Figure S1

Supplemental Figure S1: Relationship between change in neuronal response and shift in saccade endpoint.

A) Correlation between the change in neuronal response and the shift in saccade endpoint from photostimulation for saccades to a single target in one experiment. The magnitude of the saccadic shift is shown for each photostimulation trial, relative to the mean saccade endpoint during trials with no photostimulation. The change in neuronal response is also calculated relative to the control mean. The small correlation coefficient and the high p value indicate no relationship. B) Summary of correlations between saccadic shift and change in neuronal response for saccades to all targets in all experiments. For saccades to every target we have plotted the correlation coefficient versus the significance of the correlation. Note especially the marginal histogram at the top, which shows that correlations were just as likely to be positive as negative. That is, larger saccadic shifts were not necessarily accompanied by larger changes in neuronal responses. Given that we record from a small subset of the large number of neurons responsible for determining the saccade trajectory, and the modest size of the observed effects, we did not expect such a correlation to be evident. C) Summary of the same correlations for normal saccades. Small changes in neuronal response do not predict changes in saccade endpoints even in the absence of photostimulation.

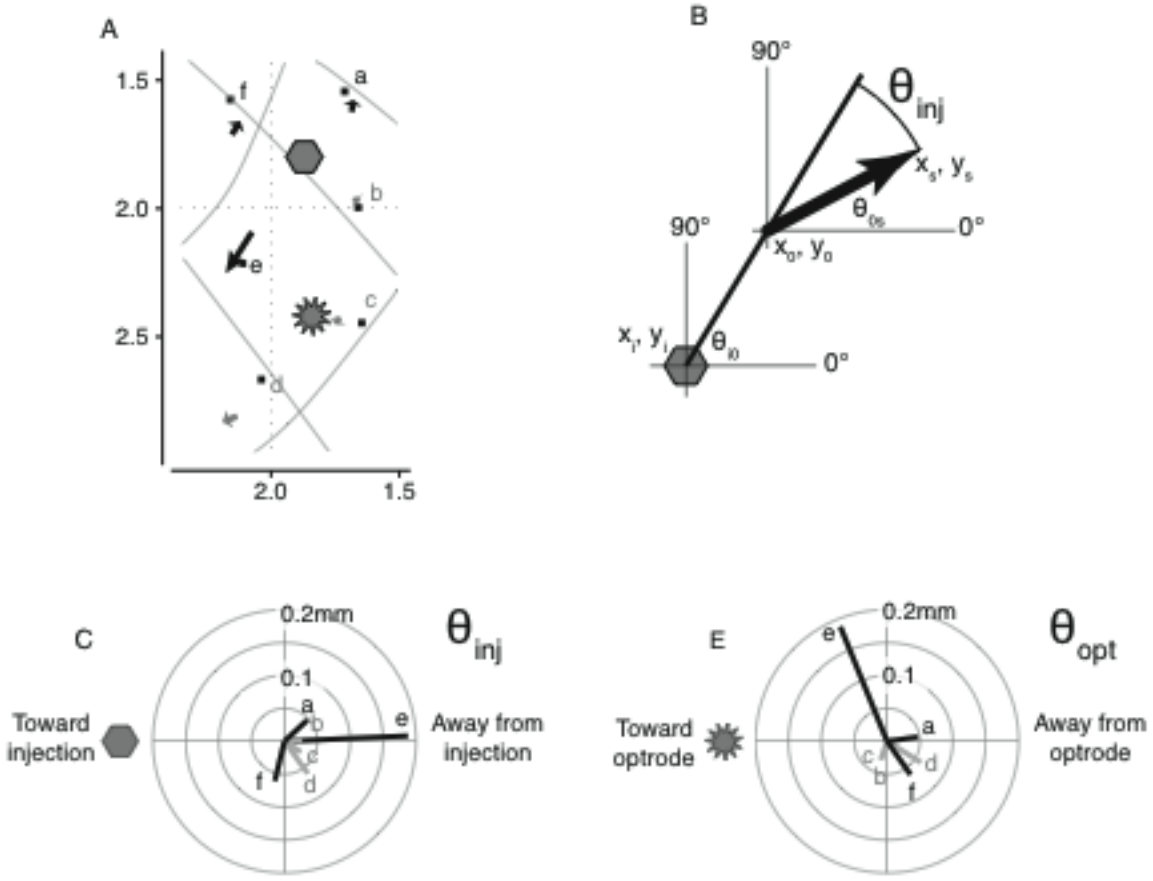
A
1.5
2.0
2.5
2.0
1.5
a
b
c
d
e
f
B
90°
θinj
xs, ys
θts
0°
90°
xo, yo
xi, yi
θio
0°
C
0.2mm
0.1
θinj
Toward injection
Away from injection
a
b
c
d
e
f
E
0.2mm
0.1
θopt
Toward optrode
Away from optrode
a
b
c
d
e
f

Figure S2

Supplemental Figure S2: Derivation of magnitude and direction of saccade deflections.

A) Same region of interest on the SC map as in Figure 2C showing shifts in saccade endpoints. B) Graphical derivation of the angle θ_{inj} representing how saccades shifted away from the injection. Complete derivation can be found in Supplemental Experimental Procedures. C) Vectors showing how the example saccade endpoints shifted away from the injection site. The vectors labeled a-f show how they correspond to the shifts in A. The length of each vector is the magnitude of the shift in mm on the SC. Significant shifts are black. D) Example vectors as in C, except this time indicating saccadic shifts away from the illuminating optrode. Again the labels a-f correspond to shifts in A.

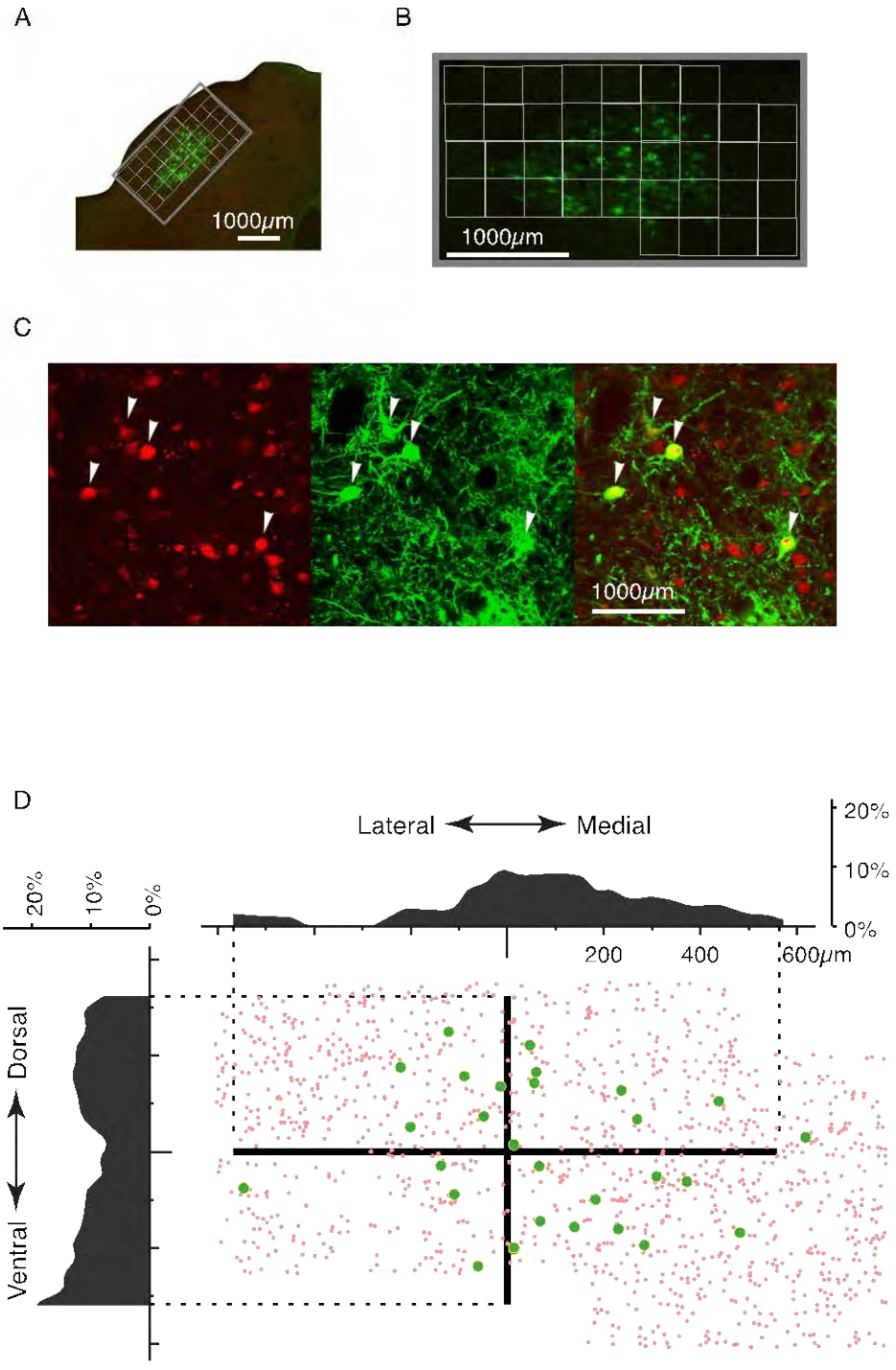
A
B
1000μm
1000μm
C
1000μm
D
Lateral
Medial
20%
10%
0%
20%
10%
0%
200
400
600μm
Dorsal
Ventral

Figure S3

Supplemental Figure S3: Histological determination of ArchT transfection.

A) Portion of a single stained coronal section from monkey RO showing GFP staining in the intermediate layers (green) of the SC. For each section, a region was chosen (the box) for confocal microscopy and cell counting. B) The box from A is enlarged, showing a grid of sub-regions. C) Representative NeuN (left), GFP (center) and double labeling (right) within the same portion of a sub-section. White arrows indicate the same transfected cells in each panel. D) Counted cells, marginal distributions of transfection, and X,Y extents of transfection for a single section. Note the extent of the counted cells corresponds with the sub-region grid from B. Cells with the NeuN stain are shown in red, and transfected cells (those also expressing GFP) are shown in green. We constructed marginal plots of the proportion of counted cells that expressed GFP (and so were also transfected with ArchT). The extreme limits of the density plots gave us an estimate of the overall spread of the transfection (as opposed to its density). The large central cross represents the overall spread of transfection in the X and Y directions derived from the limits of the density plots, as shown by the dashed lines. Refer to the box in A to assess how the X and Y axes correspond to medial-lateral and dorsal-ventral axes for this histological section.

Supplemental Experimental Procedures

Behavioral tasks and data collection

Three adult male monkeys (OZ, OM, RO, *Macaca mulatta*) provided data for different aspects of these experiments. Behavioral effects of optogenetic inactivation of the SC: monkeys OZ and OM. Mapping of interactions among injection, optrode, and target locations: monkey OZ and RO, detailed mapping, OZ. The extent of neuronal suppression on the SC map: monkeys OZ and RO. Histological analysis of injection spread: monkey RO.

Monkeys OZ and OM fixated on a central point and made visually guided saccades to a white circular target with a small black square situated in its center. The purpose of the black square was to give an unambiguous and precise endpoint for saccades, since the bright target itself could subtend several degrees of visual angle. The fixation point going off was the cue to make a saccadic response to the target. Trials with and without laser stimulation were randomly interleaved. The seven experiments performed on monkey OM involved saccades to a single target at the visual field location corresponding to the optrode site. Monkey OZ made saccades to several targets during each of 21 different experiments the number and location of which depended on the locations of the injection and the optrode. To directly compare and combine data from both monkeys, we chose the data from monkey OZ belonging to the single target closest to the optrode, but not necessarily at the optrode site, and calculated the summary statistics from saccades to those targets.

Onset of a saccade was taken as the time after the fixation point went away at which the eye exceeded a velocity of 100°/s. Changes in saccade-related neuronal activity in the SC were made by comparing the activity for a period beginning 200ms before saccade onset, and lasting 400ms.

Polar directional selectivity

We used a specific polar statistic to determine the directional selectivity of the primary behavioral effect: shift in saccade endpoint. The angle of interest θ_{inj} in Supplemental Figure S2B represents the direction of the mean shift in saccade endpoints relative to the injection site. This relative angle is the difference of the absolute angle

from the injection to the normal saccades (θ_{i0}) and the absolute angle from the normal saccade endpoints to the shifted endpoints (θ_{0s}).

We first defined the vector from the injection (x_i, y_i) to the mean of the normal saccade endpoints (x_0, y_0). This angle θ_{i0} of this vector is defined as

$$\theta_{i0} = \arctan\left(\frac{y_0 - y_i}{x_0 - x_i}\right).$$

We expressed the shift in saccade endpoints from the normal saccades (x_0, y_0) and the shifted saccades (x_s, y_s) similarly:

$$\theta_{0s} = \arctan\left(\frac{y_s - y_0}{x_s - x_0}\right).$$

The angle of deflection away from the injection is now simply:

$$\theta_{inj} = \theta_{0s} - \theta_{i0}.$$

We calculated the angle θ_{opt} similarly for displacement of saccade endpoints away from the laser illumination (the optrode site).

Viral injections

Injection of the virus was done by a custom-built injectrode assembly. First a microelectrode (FHC, Bowdoin, ME; www.fh-co.com) was glued to the side of length of 0.155mm OD silica tubing with cyanoacrylate adhesive. Next a 0.35mm OD polyimide sheath was glued over this assembly with cyanoacrylate. Finally, a drop of epoxy cement at the top of the assembly secured the parts together. The microelectrode was attached to the silica tubing such that the electrode tip extended 500µm beyond the tip of the syringe. The injectrode was passed through a guide tube that fit into a standard grid in the implanted recording cylinder (Crist et al., 1988). The guide tube was 23-gauge extra thin

wall steel tubing (ID 0.5mm). The injectrode was mounted in a custom apparatus comprising two separate stepper motors: one for lowering the entire injectrode, and one for injecting the contents of the syringe. Our apparatus allowed for slow injection rates of 0.1µl/min.

We used a construct of ArchT (Han et al., 2011) fused to GFP in an adeno-associated virus (AAV) (CAG promoter, serotype 8, synthesized by UNC Vector Core; nisi@email.unc.edu) developed by the Boyden laboratory at MIT that has been used in the mouse and the monkey. The virus was stored in a -80C freezer. An aliquot of the virus was allowed to slowly thaw in a vial in a bucket of ice. When thawed, it was drawn into the 10µl syringe of an injectrode that also was kept on ice. We were able to gauge the position of the injectrode in the SC by monitoring the visual and saccade-related neuronal activity at the tip of the attached electrode. When the electrode first reached saccade related neurons, the injectrode was lowed an additional 500µm before the injection commenced in order to put the tip of the syringe at the depth of the recorded neuronal activity. We made injections with total volumes of 6-7µl in the intermediate layers of the SC. In monkey RO the entire injection of 6µl was made at a single depth in the intermediate layers. In monkey OZ, 3.5µl was injected first, followed by another injection of 3.5µl at a depth 500µm lower for a total of 7µl. In monkey OM, the injection was again made at two separate depths in the intermediate layers of the SC, the first being 3.5µl, the second being 2.5µl 900µm lower for a total of 6µl. We waited at least six weeks after each injection before testing for sensitivity to light; we did not determine whether this interval could be shorter. We found no obvious differences in the normal activity of the SC neurons in areas with and without injections, so we see no disadvantage in using somewhat larger injection volumes injected at these slow rates.

Laser stimulation

Optrode construction was very similar to the injectrode that we used to inject the virus. First the microelectrode was glued to the side of an optic fiber with cyanoacrylate adhesive. Second a 0.45mm OD polyimide sheath was glued over this assembly with cyanoacrylate. Third, a drop of epoxy cement at the top of the assembly again secured the parts together. The optic fibers were either made from 200µm diameter fiber optic

cable with an attached fiber optic connector (Thor Labs, Newton, NJ; www.thorlabs.com), cut to size with the tip buffed, or from a 200µm diameter optic fiber with polyimide buffer, polished tip, and attached connector (Doric Lenses, Quebec, Canada; www.doriclenses.com).

Our light sources were 532nm DPSS green light lasers with a maximum power of up to 1000mW, (IkeCool Corporation, Anaheim, CA; www.ikecool.com). We measured the light intensity using an optical power meter (model 1916-C) coupled with a 818-SL/DB photo detector (Newport Corporation, Irvine, CA; www.newport.com).

For monkey RO we turned the laser on and off to illuminate the SC. Other researchers had reported large transients in light output accompanying laser onset (personal communication, John Reynolds, Salk Institute). We therefore looked at the light coming from the laser when powered on by using a custom photocell circuit connected to an oscilloscope. We found that the onset of the laser was accompanied by an initial transient pulse about ten times the steady state amplitude, and about 300ms in duration. For the other two monkeys (OZ and OM) we left the laser on continuously during the experiment and placed a mechanical shutter in the light path that had a 2mm aperture and an opening time of less than 300µs (Uniblitz model LS2, Vincent Associates, Rochester, NY; www.uniblitz.com). We designed and constructed a custom mount for the shutter, incorporating mechanical micro-positioners to align the optic fibers before and after the shutter. Even with fine adjustments of fiber alignment there was substantial light loss. However, all measurements we report were taken after the light had passed through the shutter (i.e. from the tip of the optrode). Light intensities were 650-1000 mW/mm^2 out of the fiber end.

For monkeys OZ and OM, laser light was introduced into the intermediate layers of the SC by opening the shutter placed between the laser and the optrode. For monkey OZ, the shutter opened when the fixation point went away (the cue to make a saccade) and remained open, illuminating the intermediate layers of the SC, for 500ms. For monkey OM, the shutter opened when the stimulus appeared and remained open throughout the trial (thus during the saccadic response) for 1500ms.

Data from monkey RO were acquired during free viewing. The laser was turned on in the middle of each trial, providing a period of no laser stimulation immediately followed by a period of laser stimulation. We compared neuronal activity 500ms before the laser was turned on to neuronal activity 500ms after the laser was turned on.

Histology

In monkey RO we examined the spread and efficacy of the viral injection by visualizing the GFP in histological sections, which was coupled with ArchT and served as a marker for cells with the construct. The monkey was euthanized with an overdose of pentobarbital (>70 mg/kg, i.v.). The animal was immediately perfused through the left ventricle, first with phosphate buffered saline (PBS; pH 7.4, 2 liters), then with 1% paraformaldehyde in PBS (1 liter) and with 4% paraformaldehyde in PBS (3 liters), followed by 2 liters of PBS. The brain was blocked and cryoprotected in PBS with 10% sucrose (>2 days), and then in PBS with 30% sucrose until it sank. Tissue was then cut into 50μm coronal sections on a sliding microtome and stored in PBS.

We permeabilized the slices by washing three times for 30 minutes in PBS, 100 mM glycine, and 0.5% triton X-100 (PTG solution). Slices were then incubated for 2 hours in PTG + 2% normal goat serum (Vector Laboratories, Burlingame, CA; www.vectorlabs.com) (PTB solution). The tissue was incubated with two primary antibodies: mouse anti-NeuN (1:1000, Chemicon Intl., Temecula, CA; www.chemicon.com) and chicken anti-GFP (ab13970, 1:3000 - Abcam, Cambridge, MA; www.abcam.com) in PTB overnight at 4C on shaker. The primary antibody was washed off 4x30 minutes with PTG solution. Then the tissue was incubated with secondary antibodies in PTB solution for 2 hours at room temperature on shaker. The secondary antibodies were Alexa 594 goat anti-mouse, 1:500, (A11032; Invitrogen, Grand Island, NY; www.invitrogen.com), and Alexa 488, goat anti chicken, 1:100 (Invitrogen A11039). After we washed of the excess secondary antibodies, the slices were mounted with Vectashield solution (Vector Labs, Burlingame, CA: www.vectorlabs.com) and visualized by confocal microscopy.

Confocal microscopy and cell counting

Tissue was stained for both NeuN and GFP. We imaged eleven sections separated by 250μm and subtending the anterior-posterior extent of the injection. Confocal microscopy produced a series of digital images at different depths for both stains within each histological section. Each section was divided into a grid of sub-regions encompassing the apparent extent of the injection in each section, with each sub-region subtending 318μm square. Supplemental Figure S3A shows the location of the injection in monkey RO on a coronal section through the left half of the SC. The box in Figure S3A shows the area selected for confocal microscopy and subsequent counting of transfected cells. Supplemental Figure S3B shows the grid used to divide each 50μm thick section of the SC into sub-regions for confocal microscopy within the box from Figure S3A. We objectively determined a single confocal depth for cell counting separately for each sub-region by finding the depth at which the mean luminance of the NeuN stain in the sub-region was greatest (an objective measure of the best neuronal expression).

Once we located the depth in each section expressing the strongest NeuN stain, we counted neurons stained with NeuN using ImageJ (Rasband, 1997). We then counted those cells that also expressed GFP, indicating cells transfected with ArchT. Part of a sub-region is shown in Supplemental Figure S3C, showing examples of the images used for counting transfected cells. The left panel shows the NeuN stain for neurons, the middle panel shows the GFP stain for viral transfection, and the right panel shows the overlap of the two in which cell bodies stained for GFP appear yellow (white arrows). We kept track of not only the cell counts, but also the location in the grid of each counted cell. This allowed us to reconstruct the location of each neuron and each transfected neuron in two dimensions for each slide (the central scatterplot in Supplemental Figure S3D). Counted neurons are red, and neurons that also stained for GFP are green. We expressed the degree of transfection along both the X and Y axes of each section as a running mean. We first estimated the peak region of transfection by calculating the running mean within a 500μm window for the number of counted neurons separately for the X and Y axes. We smoothed the resulting curve with a wide Gaussian (50μm SD) and did the same for cells expressing GFP. The ratio of the two smoothed counts gave us an initial estimate of the level of ArchT transfection along the X and Y axes. We located the peak density along the

X axis and recalculated the running means for the Y axis using only cells within 250µm of the X peak. We did the same for the Y axis peak to obtain running means along the X axis. In effect this removed the transfection-sparse margins along each dimension before calculating the peak transfection in each section. These final running means were again calculated with a 500µm window, only this time smoothed with a narrower Gaussian (25µm SD). The marginal average density plots have had the peripheral 100µm removed to reduce overestimation of the extent of transfection introduced by the width of the running mean window. These density plots represent the approximate overall spread in the X and Y directions, as represented by the dimensions of the large central cross. This central cross representing the X and Y extents of transfection was used to create the three dimensional reconstruction of the injection in Figure 4C. The example marginal density plots in Supplemental Figure S3D are indicated by a darker shade in Figure 4C.

Supplemental References

Crist, C.F., Yamasaki, D.S., Komatsu, H., and Wurtz, R.H. (1988). A grid system and a microsyringe for single cell recording. J Neurosci Methods 26, 117-122.

Rasband, W.S. (1997). Image J (National Institutes of Health, Bethesda, Maryland, USA).